Investigating Deformation in HDPE-Wood Flour Composites Using Uniaxial Tension and Nanoindentation Experiments

Joseph E. Jakes, Nathan J. Bechle, Scott Hamel, Arthur G. Gronvold, John C. Hermanson, and Donald S. Stone

Abstract

Deformation properties of a high-density polyethylene (HDPE)-wood flour composite were investigated using uniaxial tension and nanoindentation experiments. Before composite failure under tension, the composite exhibited qualitative behavior and flow-stresses similar to those of neat HDPE. However, the composite failed at low strains (~0.03) and did not exhibit the necking process characteristic of neat HDPE. Nanoindentation techniques, producing indents less than 10 µm across, are capable of probing the properties of the HDPE matrix within the composite. Using our broadband nanoindentation creep (BNC) method, we measured instantaneous hardness (H) of the HDPE matrix over four decades of indentation strain-rate (10^{-3}–10^{1}). At the lowest strain rate, H ranges from 60 to 90 MPa; at the highest strain rate, H increases up to 200 MPa. The H data were converted to uniaxial flow-stress data and compared to yield-stress data determined from tensile experiments performed on the composite. Differences between the nanoindentation-based uniaxial flow-stress and tensile uniaxial yield-stress data can be explained in part by the role of hydrostatic pressure beneath the indenter.

Jakes:
Materials Research Engineer, USFS Forest Products Laboratory, Madison, Wisconsin, USA

Bechle:
Research Assistant, USFS Forest Products Laboratory, Madison, Wisconsin, USA

Hamel:
Research Assistant, USFS Forest Products Laboratory, Madison, Wisconsin, USA

Gronvold:
Former Research Assistant, USFS Forest Products Laboratory, Madison, Wisconsin, USA

Hermanson:
Research Engineer, USFS Forest Products Laboratory, Madison, Wisconsin, USA

Stone:
Professor, Dep. of Materials Science and Engineering, University of Wisconsin–Madison, Madison, Wisconsin, USA

Introduction

Properties of a composite material are controlled by the properties of its components and interactions between the components. However, how the different components interact and contribute to the composite properties is not well understood. The high-density polyethylene (HDPE)-wood flour composite we studied consists of wood particles that ranged in size from sub-micrometer (cell wall fragments) to hundreds of microns (groups of intact cells), embedded in a matrix of melt-crystallized HDPE. Additional components, including a coupling agent, were also included in the composite. In this investigation we considered the contributions of HDPE to the behavior of the composite by comparing the uniaxial tensile behavior of the composite both to the uniaxial tensile behavior of neat HDPE and to properties of the HDPE regions of the composite measured in situ by nanoindentation. The goal of this research is to provide insight into which composite properties are controlled by the HDPE component so researchers can better understand how changing the properties of the HDPE component affect the composite properties.

Understanding the properties of neat HDPE provides the foundation for understanding our HDPE–wood flour composite. HDPE in the solid state is a semi-crystalline polymer consisting of crystalline and amorphous domains. The morphology of HDPE depends on the properties of the starting material (e.g., molecular weight distribution), whether the HDPE is crystallized from solution or melt-crystallized, and conditions during crystallization (e.g., rate of crystallization or applied pressure during crystallization). Typical melt-crystallized HDPE possesses a spherulitic morphology with spherulites on the order of 100 µm in diameter. Crystalline domains are composed of folded chains and organized in lamellae of ~20 nm thickness. The lamellae are surrounded by amorphous domains composed of tie molecules connecting neighboring lamellae and entangled loose ends and loops (Lin and Argon 1994 and citations therein).

Deformation of neat HDPE is a complex, multistage process. The role of the amorphous and crystalline phases varies depending on the deformation stage. At strains less than about 0.05, deformation is mostly recoverable and occurs in the amorphous domains (Bartczak et al. 1992). At room temperature, the amorphous material is above its glass transition temperature and deforms in a rubber-like manner. At strains higher than about 0.05, the crystalline lamellae also begin to plastically deform (Bowden and Young 1974, Bartczak et al. 1992). The crystallographic deformation proceeds primarily by dislocations with Burgers vectors either parallel or perpendicular to the chain axis (Lin and Argon 1994). The critical resolved shear stresses for the different slip systems vary from 7.2 to 15.6 MPa, and unlike typical crystalline materials, such as metals, the critical resolved shear stresses in crystalline polymers possess a substantial pressure dependence (Lin and Argon 1994).

Experimental Methods

Materials

A composite composed of an HDPE matrix and wood flour was used in this work. The composite formulation consisted of 55% (by weight) wood pine flour, 30% HDPE, and 2% proprietary coupling agent. The composite was manufactured by the Strandex Corporation (Madison, WI), and the remaining 13% of the composite and details about the extrusion process are proprietary.

Nanoindentation Experiments

To prepare the nanoindentation specimen, we first cut a 10 mm cube from the extruded board. The cube was mounted in a sledge microtome equipped with a disposable microtome blade and a gently sloping (~15°) apex was microtomed on the surface, oriented perpendicular to the extrusion direction. The specimen was then fitted into an ultramicrotome equipped with a diamond knife and the tip of the apex was cut off, revealing a surface suitable for nanoindentation experiments. Only one nanoindentation specimen was prepared.

Nanoindentation experiments were performed with a Hysitron (Minneapolis, MN) Triboindenter equipped with a Berkovich tip and operated in force control. The load function consisted of a multiload portion, 60-s thermal drift segment, and 50-s creep segment at a maximum load of 1 mN [see Fig. 4 in Jakes et al. (2009) for more detail]. Six indents were placed in the HDPE matrix of the composite. Residual indents were imaged with a Quesant (Agoura Hills, CA) atomic force microscope (AFM) incorporated in the Triboindenter. The AFM was operated in contact mode and calibrated using an Advanced Surface Microscopy, Inc. (Indianapolis, IN), calibration standard with a pitch of 292 ± 0.5 nm. Individual 15-µm field of view images were made of each indent, and ImageJ (onta://rsb.info.nih.gov/ij/; verified 21 Dec. 2009) image analysis software was used to manually measure the projected contact areas as described in our previous publications (Jakes et al. 2008, 2009). From the multiload portion of the load-depth trace, SYS correlations were constructed and the load-depth traces were corrected for any structural compliances arising from specimen-scale flexing or edge effects (Jakes et al. 2008, 2009). The load-depth traces were also corrected for thermal drift using the thermal drift segment (Jakes et al. 2008, 2009). From the creep segment, instantaneous hardness (H) and indentation strain-rate were determined using the broadband nanoindentation creep (BNC) analysis outlined in Puthoff et al. (2009). A value of 1.12 was used for the power law exponent ξ_p in the BNC analysis when calculating area as a function of depth during creep.

Uniaxial Tension Experiments

The uniaxial tension experiments were conducted according to ASTM D 638 (The Standard Test Method for Tensile Properties of Plastics) (ASTM 2002). The specimens were type I dog-bone specimens cut from the extruded boards and machined to size. The orientation of the specimens was such that the uniaxial stresses would be aligned with the extrusion direction. Dog-bone specimens were tested in a servo-hydraulic MTS Systems Corp. (Eden Prairie, MN) testing machine. Specimens were gripped using rigid steel U-shaped mechanical grips with serrated swivel pads secured to bolts. The actuator was controlled with an MTS 407 controller box with the head displacement measured using a Trans-Tek Series 240 (Trans-Tek, Inc., Ellington, CT) linearly variable differential transducer (LVDT). The tests were displacement controlled using the output from the LVDT as feedback. Specimen displacements were measured using an Instron extensometer (Model 2630–004) (Instron Corp., Norwood, MA) with a 1-in. gauge length. Load measurements were achieved with a 2000-lbf Sensotec load cell (Model 41/572–01) (Honeywell Sensotec, Columbus, OH). Data were acquired using a custom-written LabVIEW program sampling at various rates depending on the speed of the test. Experiments were conducted at strain rates of 0.03, 0.1, 1, 10, and 100% strain/min with five to nine replicates per strain rate.

Results

Nanoindentation Experiments

A representative load-depth trace of an indent placed in the HDPE matrix of the composite is shown in **Fig. 1**, and the corresponding AFM image is shown in **Fig. 2**. Indents were carefully placed to not overlap the larger (micrometer-size) cell wall fragments in the matrix; however, it was not possible to avoid the sub-micrometer-size particles embedded in the matrix. The effect of sub-micrometer-size particles on the Meyer's hardness (defined as maximum load divided by contact area) changed for each indent depending on the number and size of particles directly under the indenter. Differences in proximity of the indent to the larger cell wall fragments could have also affected the hardness. In previous work we found that the hardness was affected when the ratio of the square root of contact area to the distance of a free edge to the center of the indent was greater than 0.8 in polymethylmethacrylate (PMMA) (Jakes et al. 2009). The effects of the submicrometer-size particles and proximity of larger cell wall fragments contributed to the scatter in the six H vs. indentation strain-rate ($\dot{\varepsilon}_H$) curves in **Fig. 3**. These curves were calculated using the methods outlined in Puthoff et al. (2009). The data spanned four decades of $\dot{\varepsilon}_H$ (10^{-3}–10^{-1}); at the lowest $\dot{\varepsilon}_H$, H ranged from 60 to 90 MPa, and at the highest $\dot{\varepsilon}_H$, H increased to the range of 150 to 200 MPa. To compare the H–$\dot{\varepsilon}_H$ data to the forthcoming uniaxial data, the curves were converted to effective uniaxial flow-stress (σ^{eff}) versus effective uniaxial strain-rate ($\dot{\varepsilon}^{eff}$) using the method outlined in Puthoff et al. (2009). The analysis assumed an effective indentation modulus of 1.6 GPa for HDPE, which was determined in our preliminary nanoindentation experiments to determine the modulus of the matrix phase.

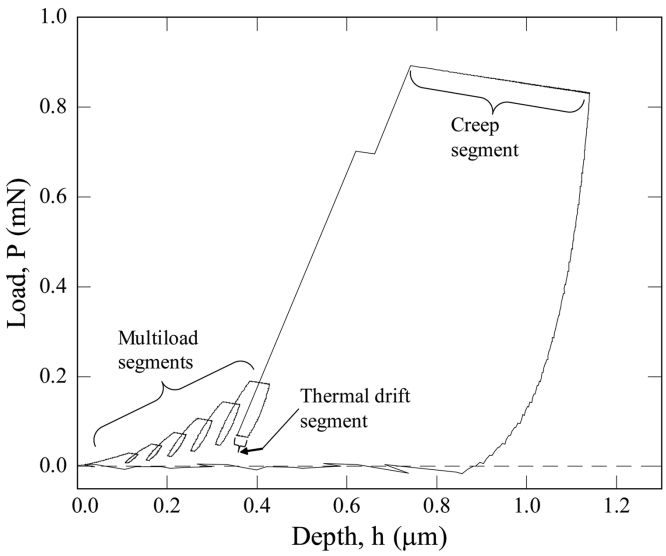

Figure 1. ~ *Representative load-depth trace of an indent placed in the matrix of the HDPE-wood flour composite.*

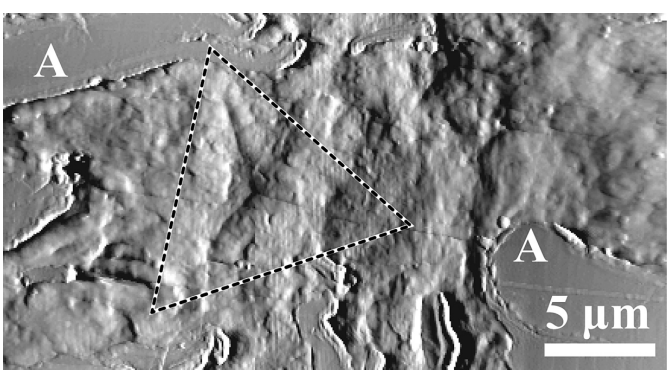

Figure 2. ~ *Atomic force microscope image of an indent placed in the matrix of the HDPE-wood flour composite. The indent was placed to not overlap the larger micron-sized cell wall fragments (A). The triangle closely outlines the contact edges of the indent but is not meant to be exact.*

Uniaxial Tension Experiments

A representative stress (σ) versus strain (ε) curve for the uniaxial tension experiments is shown in **Fig. 4**. The yield stress (σ_y) was determined at a 0.005 offset from the σ–ε curve as illustrated in **Fig. 4**. The modulus of elasticity (MOE) used to determine the elastic component of the strain was calculated by fitting the σ–ε curve up to the maximum stress to the hyperbolic sine function

$$\sigma = A\sinh^{-1}(B\varepsilon) + C\varepsilon \qquad [1]$$

where A, B, and C are fitting parameters. The MOE was defined as the derivative of this fit at ε = 0. To determine $\dot{\varepsilon}^{eff}$ at the determined σ_y, the slope of the ε vs. time curve was determined at the ε corresponding to the σ_y. The resulting σ_y–$\dot{\varepsilon}^{eff}$ data from the uniaxial tension experiments are also plotted in **Fig. 3**. In addition, values of σ_y for uniaxial tension found in the literature for neat HDPE are also included in **Fig. 3**. In Andrews and Ward (1970), s_y was defined at the "yield" point, with no further detail given. In Gent and Madan (1989), σ_y was defined as the maximum stress achieved before the drawing stress.

Discussion

The properties of HDPE are modified with the addition of wood flour, coupling agent, and other materials. The σ–ε curve of the HDPE–wood flour composite in **Fig. 4** is less ductile than the neat HDPE σ–ε curve in the inset of **Fig. 4**. At low strains, the σ–ε curve for neat HDPE is similar to our composite σ–ε curve but fails at a factor of 100 higher strain than the composite. As the strain increases, the neat HDPE curve deforms by necking at a nearly constant stress, called the drawing stress, which is similar in value to the yield-stress. After the necking deformation process is exhausted, stress begins to increase until failure at strains that commonly approach a value of two (Lin and Argon 1994). The difference in σ–ε behavior between the neat HDPE and the composite

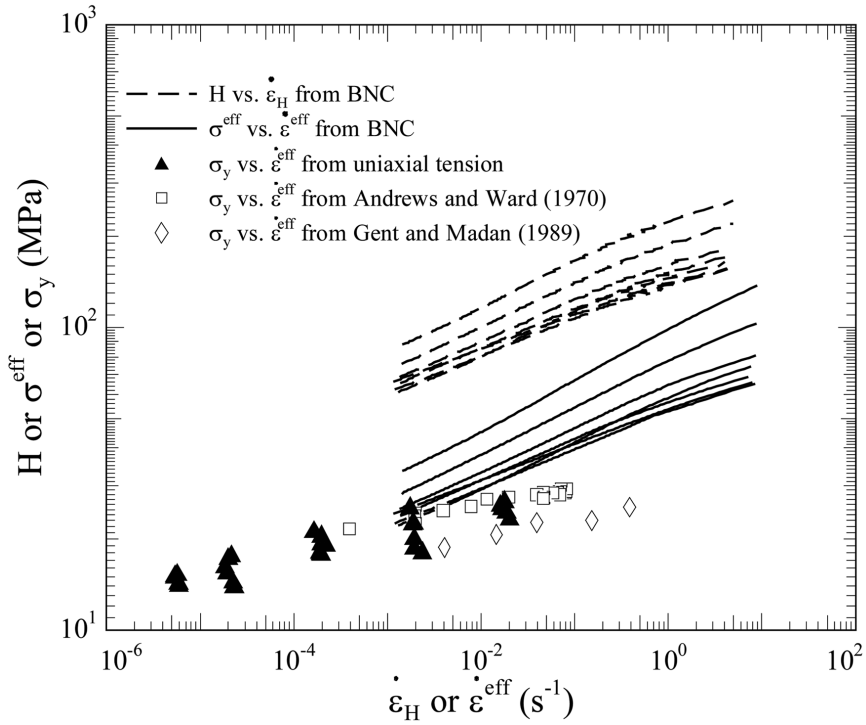

Figure 3. ~ *Instantaneous hardness (H) vs. indentation strain-rate ($\dot{\varepsilon}_H$) and broadband nanoindentation creep (BNC)-generated uniaxial flow-stress (σ^{eff}) vs. uniaxial strain-rate ($\dot{\varepsilon}^{eff}$). Also plotted are yield-stress (σ_y) vs. $\dot{\varepsilon}^{eff}$ data from uniaxial tension experiments on HDPE-wood flour composite and σ_y–$\dot{\varepsilon}^{eff}$ data from the literature for neat HDPE uniaxial tension experiments.*

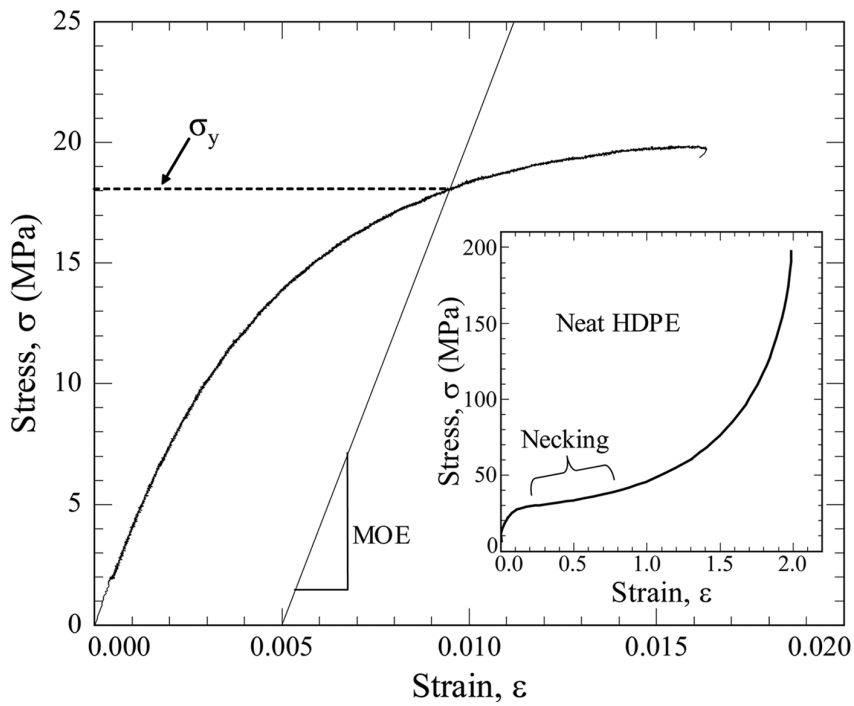

Figure 4. ~ *Representative stress (σ) vs. strain (ε) curves from an HDPE-wood flour composite uniaxial tension experiment. Inset: Representative σ–ε curve for neat HDPE taken from Lin and Argon (1994). Note the abscissa for the inset goes to a strain of two.*

is caused by the addition of the wood flour phase and possible changes in the morphology of the HDPE in the composite. We suspect that the regular spherulitic structure and percentage crystallinity of HDPE are modified by the wood flour, coupling agent, and other materials in the composite. Despite differences in the ductile behavior exhibited in the σ–ε curves of the HDPE and composite, our values of σ_y for the HDPE-wood flour composite experiments are similar to the literature values for neat HDPE (Andrews and Ward 1970, Gent and Madan 1989). This suggests that deformation of the HDPE and the composite at low strains is controlled by similar mechanisms, likely deformation of the amorphous domains in HDPE, and this deformation is not affected by the additional material in the composite.

We performed BNC experiments to investigate the flow properties of the matrix phase in a HDPE–wood flour composite. However, BNC data are not directly comparable to uniaxial data. The effective strain under a Berkovich indenter is 0.08 (Tabor 1970), which is higher

than the strain reached in the uniaxial experiments, and therefore different deformation mechanisms may be controlling the results. Nevertheless, the method outlined in Puthoff et al. (2009) was employed in this work to convert BNC data to uniaxial data for comparison with experimental uniaxial data. The σ^{eff}– $\dot{\varepsilon}^{eff}$ data generated from nanoindentation (six solid curves in **Fig. 4**) have a steeper slope than the data from the uniaxial experiments on bulk specimens, which is similar to the difference between nanoindentation data and uniaxial data reported in experiments performed on PMMA by Puthoff et al. (2009). Those authors attributed the difference to the effect of hydrostatic pressure on the flow under the indenter and quantified the effect in terms of a pressure activation volume. The similarity between the earlier results on PMMA and the behavior of our data here also suggests that nanoindentation data from the HDPE in the composite are affected by hydrostatic pressure. The hydrostatic pressure effect is consistent with the generally observed pressure dependence of flow in solid polymers (Ward 1971) and more specifically here with the reported pressure dependence of the critically resolved shear stress in the deformation of the crystalline regions of HDPE (Lin and Argon 1994). We are currently refining our methods to convert BNC data to uniaxial data and take the hydrostatic pressure into account so more meaningful comparisons can be made between BNC and uniaxial experiments.

Conclusion

Uniaxial tension and BNC experiments were performed on an HDPE-wood flour composite. Comparing our experimental uniaxial data to literature uniaxial tension data on neat HDPE revealed a similar shape at low strains, and values of yield-stress were similar between the neat HDPE and composite. This suggests the HDPE component controls the initial yielding of the composite. However, the composite was less ductile than neat HDPE and failed at two orders of magnitude lower strain. Nanoindentation was capable of probing the flow properties of the matrix in the HDPE–wood composite in situ. However, the comparison between BNC and uniaxial data is not straightforward, a result that we attribute in part to an effect caused by the hydrostatic pressure beneath the indenter.

Literature Cited

Andrews, J.M., and I.M. Ward. 1970. The cold-drawing of high density polyethylene. J. Mater. Sci. 5:411–417.

ASTM. 2002. ASTM D 638–02a. Standard test methods for tensile properties of plastics. American Society for Testing and Materials, West Conshohocken, PA.

Bartczak, Z., R.E. Cohen, and A.S. Argon. 1992. Evolution of the crystalline texture of high-density polyethylene during uniaxial compression. Macromolecules 25:4692–4704.

Bowden, P.B., and R.J. Young. 1974. Review: Deformation mechanisms in crystalline polymers. J. Mater. Sci. 9:2034–2051.

Gent, A.N., and S. Madan. 1989. Plastic yielding of partially crystalline polymers. J. Polym. Sci. Pol. Phys. 27:1529–1542.

Jakes, J.E., C.R. Frihart, J.F. Beecher, R.J. Moon, P.J. Resto, Z.H. Melgarejo, O.M. Suárez, H. Baumgart, A.A. Elmustafa, and D.S. Stone. 2009. Nanoindentation near the edge. J. Mater. Res. 24(3):1016–1031.

Jakes, J.E., C.R. Frihart, J.F. Beecher, R.J. Moon, and D.S. Stone. 2008. Experimental method to account for structural compliance in nanoindentation measurements. J. Mater. Res. 23(4):1113–1127.

Lin, L., and A.S. Argon. 1994. Review: Structure and plastic deformation of polyethylene. J. Mater. Sci. 29:294–323.

Puthoff, J.B., J.E. Jakes, H. Cao, and D.S. Stone. 2009. Investigation of thermally activated deformation in amorphous PMMA and Zr-Cu-Al bulk metallic glasses with broadband nanoindentation creep. J. Mater. Res. 24(3):1279–1290.

Tabor, D. 1970. The hardness of solids. Review of Physics in Technology 1:145–179.

Ward, I.M. 1971. Review: The yield behaviour of polymers. J. Mater. Sci. 6:1397–1417.

Tenth International Conference on Wood & Biofiber Plastic Composites and Cellulose Nanocomposites Sysmposium, May 11-13, Madison, WI. Madison, WI : Forest Products Society, c2010. ISBN 978-1-892529-55-8.